A General Strategy to Stabilize the 1T-MoS$_2$ by Using MXene Heterostructures and Unlock Its Hydrogen Evolution Reaction Capabilities

Yumiao Tian [1], Xiaochun Liu[1], Pengfei Hou[1], Yu Xie[1], Fei Du[1], Gang Chen[1], Aleksandra Vojvodic[2], and Xing Meng [1, 2, 3]*

[1] Key Laboratory of Physics and Technology for Advanced Batteries (Ministry of Education), College of Physics, Jilin University, Changchun 130012, P. R. China

[2] Department of Chemical and Biomolecular Engineering, University of Pennsylvania, Philadelphia, Pennsylvania 19104, United States of America

[3] Key Laboratory of Symbolic Computation and Knowledge Engineering of Ministry of Education, Jilin University, Changchun 130012, P. R. China

* Authors to whom any correspondence should be addressed.

E-mail: mengxing@jlu.edu.cn (Xing Meng)

Table S1. The lattice constant of the heterostructure

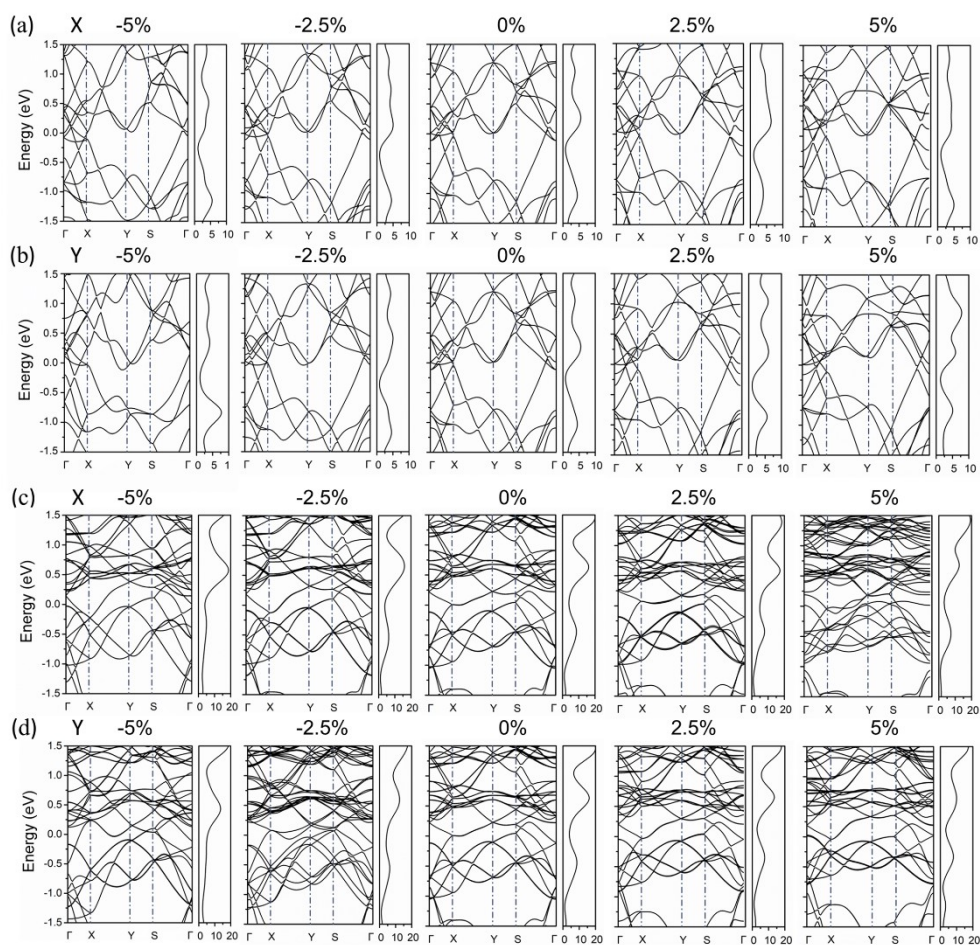|	1T-MoS$_2$-V$_2$CO$_2$	2H-MoS$_2$-V$_2$CO$_2$	1T-MoS$_2$-Mo$_2$CO$_2$	2H-MoS$_2$-Mo$_2$CO$_2$	1T-MoS$_2$-V$_2$NO$_2$	2H-MoS$_2$-V$_2$NO$_2$	1T-MoS$_2$-Nb$_2$CO$_2$	2H-MoS$_2$-Nb$_2$CO$_2$
a$_h$ (Å)	9.938	9.893	9.902	9.852	9.928	9.917	9.378	9.421
b$_h$ (Å)	5.732	5.714	5.713	5.731	5.735	5.722	5.427	5.433

Figure S1. Electronic structures under different tensile strains. 1T-MoS$_2$: (a) and (b); V$_2$CO$_2$: (c) and (d).
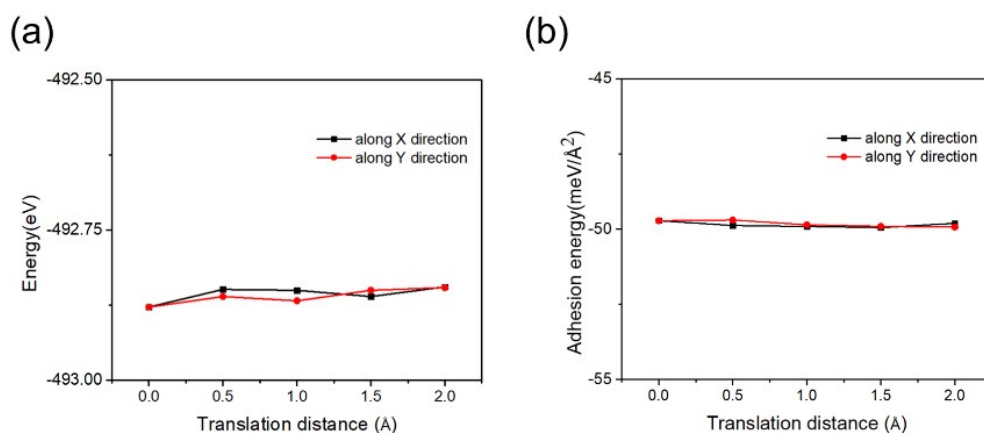

Figure S2. During the slipping process, (a) changes in the energy of the heterostructure system, and (b) changes in the interlayer binding energy of the heterostructure.
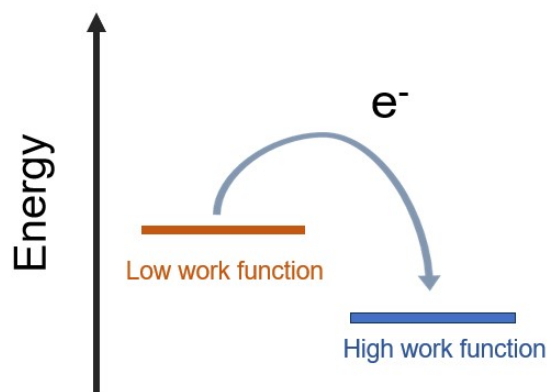
Figure S3. Schematic diagram of electron injection in the heterostructure

Table S2. Work Functions of MoS_2 and metallic MXenes with M_2XT_2 composition

	Work Function （eV）
1T-MoS_2	5.060
2H-MoS_2	5.712
V_2CO_2	6.695
Nb_2CO_2	5.820
Ta_2CO_2	5.413
Cr_2CO_2	8.010
Mo_2CO_2	7.402
Ti_2NO_2	5.989
V_2NO_2	6.135
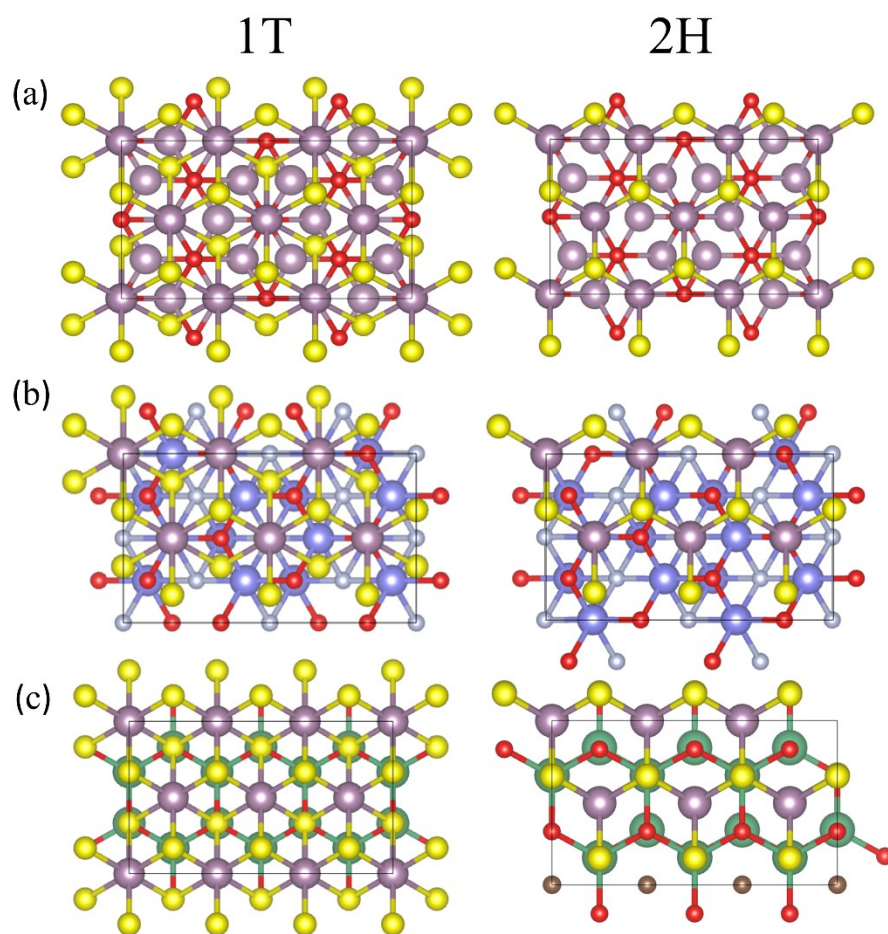
Figure S4. Top view of (a) MoS_2-Mo_2CO_2, (b) MoS_2-V_2NO_2, and (c) MoS_2-Nb_2CO_2. Color code: S, yellow; Mo, purple; Nb, green; O, red; V, blue; C, brown; and N, grey.

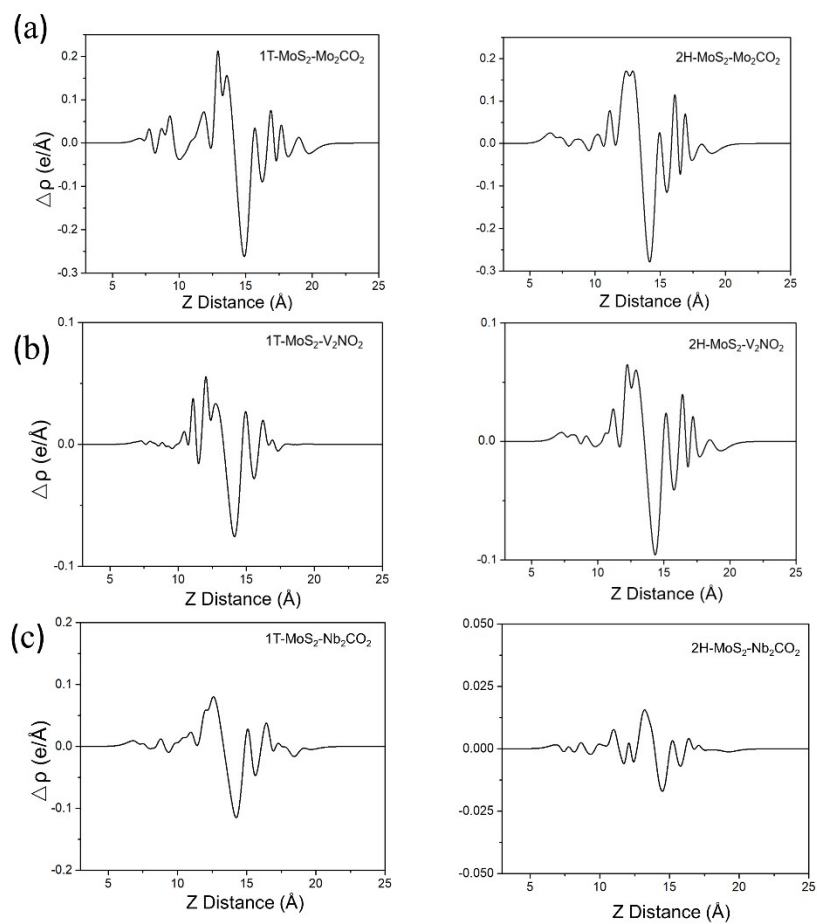**Figure S5.** Heterostructures plane-averaged charge density difference (a) MoS_2-Mo_2CO_2, (b) MoS_2-V_2NO_2, and (c) MoS_2-Nb_2CO_2

Table S3. Electron change of MoS_2 in different heterostructures

	1T-MoS_2-Mo_2CO_2	2H-MoS_2-Mo_2CO_2	1T-MoS_2-V_2NO_2	2H-MoS_2-V_2NO_2	1T-MoS_2-Nb_2CO_2	2H-MoS_2-Nb_2CO_2
Electron change of MoS_2 (e)	-0.271	-0.295	-0.061	-0.099	-0.121	-0.015

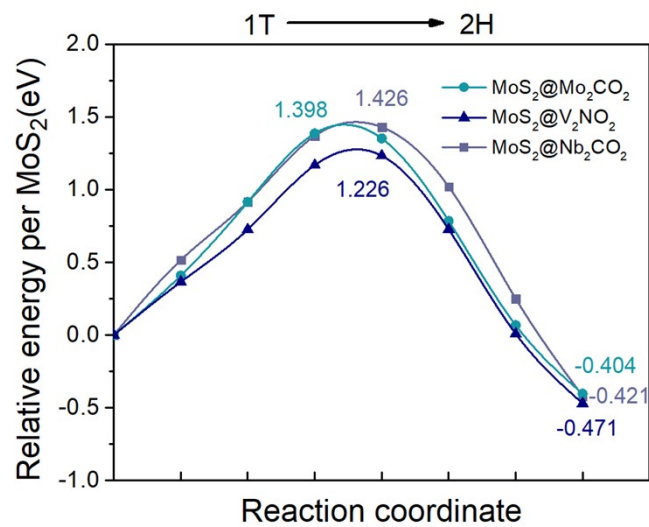**Figure S6.** Phase transition energy barrier of MoS$_2$ from 1T phase to 2H phase
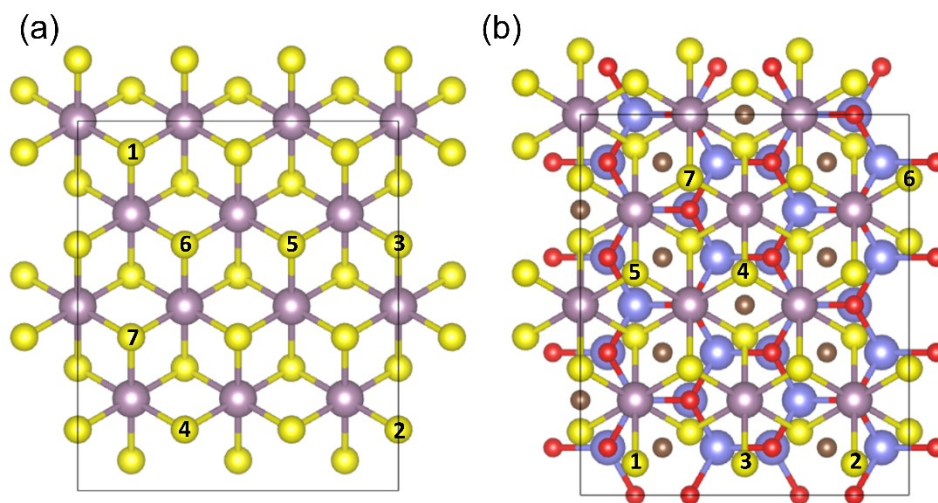

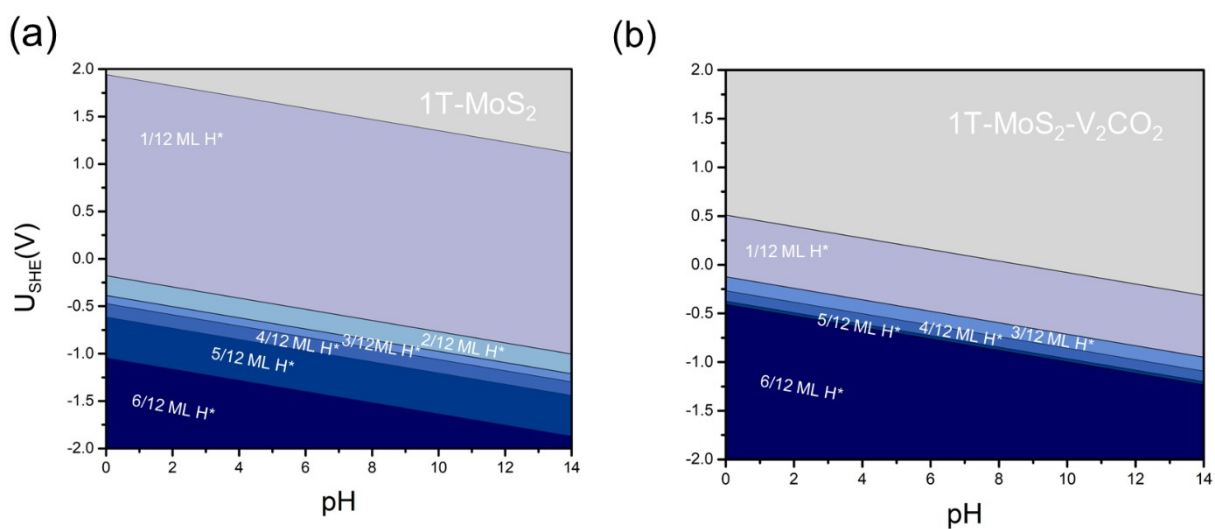**Figure S7.** Hydrogen adsorption sequence (a) monolayer 1T-MoS$_2$ and (b)1T-MoS$_2$-V$_2$CO$_2$

Figure S8. Pourbaix diagram of 1T-MoS2 under HER conditions (a) monolayer 1T-MoS$_2$ and (b)1T-MoS$_2$-V$_2$CO$_2$
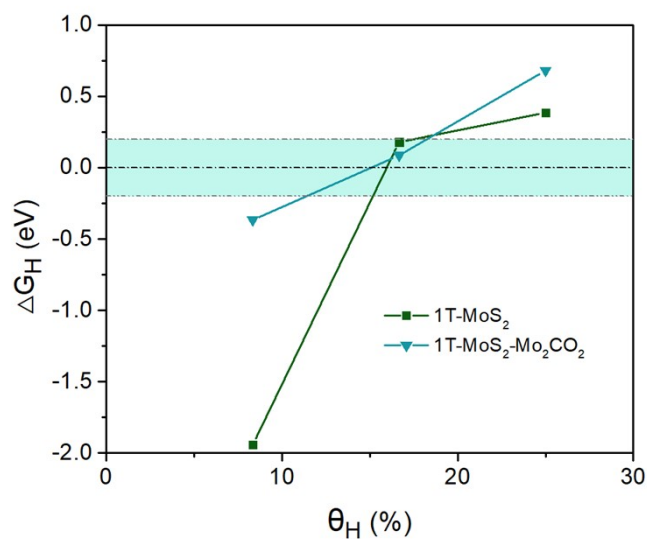

Figure S9. The hydrogen adsorption free energy at different active sites on the basal plane of 1T-MoS$_2$-Mo$_2$CO$_2$ as a function of hydrogen coverage was investigated using structures of the same size as shown in Figure S4. The optimal ΔG_H of 0.086 eV was achieved at a hydrogen coverage of 16.67%.